Optimal modification of poly(vinylidene fluoride) membrane surface by using surface-modifying macromolecules for application in membrane distillation

Reshad Shoaie[a], Javad Karimi-Sabet[b,*], Seyed Mohammad Ali Mousavian[a], Parissa Khadiv-Parsi[a], Rasoul Moradi[a]

[a]College of Chemical Engineering, School of Engineering, University of Tehran, Tehran, Iran, Tel. +982177797714; email: r.shoae@gmail.com (R. Shoaie)
Tel. +982166498982; email: moosavian@ut.ac.ir (S.M.A. Mousavian), Tel. +982166498982; email: kparsi@ut.ac.ir (P. Khadiv-Parsi),
Tel. +982166957786; email: rmoradi@ut.ac.ir (R. Moradi)
[b]NFCRS, Nuclear Science and Technology Research Institute, Tehran, Iran, Tel. +982188221117; email: j_karimi@alum.sharif.edu

abstract

The optimal engineering of the surface properties was performed for poly(vinylidene fluoride) (PVDF) membrane with hydrophobic surface-modifying macromolecules (SMMs). For this aim, new hydrophobic SMM additives were synthesized using polyurethane chemistry and characterized for water contact angle, fluorine content and average molecular weight. Both modified PVDF/SMM and neat PVDF membranes were prepared through phase inversion method in a single casting step and characterized by means of scanning electron microscope, energy-dispersive X-ray spectroscopy and contact angle goniometry. The optimum preparation conditions were determined using response surface methodology. The effects of the main casting variables, such as PVDF concentration, SMM concentration and solvent evaporation time, on the surface properties of the synthesized membrane were identified and used to prepare optimal PVDF/SMM membrane. The prepared membranes were tested for permeation flux and salt rejection efficiency by membrane distillation process. The results indicate that the optimally modified membrane yields high permeate flux of around 17.5 kg/m²h and total salt rejection efficiency of 99.9 % compared with pristine membranes. In particular, the hydrophobicity of the modified membrane significantly increases up to 108° at water contact angle, through presented surface modification procedure.

Keywords: Surface-modifying macromolecules; Poly(vinylidene fluoride); Membrane modification; Membrane distillation; Response surface methodology

1. Introduction

Surface as an interface between the bulk of the materials and the environment is the very active research area due to its straight influence on the many observable and applicable properties of substances. Especially, the surface of the polymeric materials plays the key role to determine the very specific features such as wettability, roughness, adhesion, durability, biocompatibility, etc. [1–4]. For instance, in the field of membrane science, the surface properties of the polymeric membranes recognize the class of application namely nanofiltration, microfiltration, reverse osmosis, membrane distillation (MD), etc. [5]. However, the pristine surface of the membrane sometimes dose not satisfy the desired performance [6,7]. Therefore, the required properties of the membrane surface often demand special molecular structures, which could not be fulfilled by the employed polymer chemical structure [8–10]. This is an important issue in the new emerging process of MD, for which the appropriate commercial membranes are not provided [11]. Accordingly, the treatment of the polymeric membranes especially for the MD membranes is still challenging field of investigation [12,13].

* Corresponding author.

It is well documented that the membrane surface chemistry determines its intrinsic hydrophobicity [14–16]. Hydrophobic membranes are usually made using hydrophobic polymers, e.g., polytetrafluoroethylene (PTFE) and poly(vinylidene fluoride) (PVDF), to provide the water contact angle (CA) higher than 90° [17]. This property of MD membrane prevents liquid passing through the pores and keeps them dry during the process, which enhances the operational durability.

Furthermore, the membrane casting conditions effectively influence the ultimate membrane surface and bulk structures. In addition, the introducing various additives in polymer cast solution has also the main impact on the membrane surface properties. Surface-modifying macromolecules (SMMs) are fluorinated polyurethanes comprising an amphipathic structure, which theoretically consist of a main polyurethane chain terminated with two low polarity polymer chains (fluorine segments; Fig. 1(a)). These F-containing agents are intensively used to obtain the favored properties of the membrane surface [18–20]. Design concept of SMM agents is based on polyurethane chemistry. As depicted in Fig. 1(a), the main polymer chain is synthesized by polymerization reaction of diisocyante and polyol precursors in the stoichiometric ratio. The appropriate fluoroalcohol is used as the end-capping agent and must be added to the reaction vessel before completion of the polymerization process. Thereby, the SMM oligomers could be designed by setting the factors such as the polyalcohol chemical structure and the fluoroalcohol addition time.

SMMs addition transforms the membrane into a composite bilayered form with dual characteristics. In fact, SMMs migrate to the membrane's top surface, inducing higher hydrophobicity compared with the bulk of the membrane and bottom side (Fig. 1(b)). This is due to the upward orientation of the SMM's terminal fluorine groups in the surface of the casted polymer/SMM blend solution. In addition, the morphological difference (skin top layer and porous sublayer) is created across the membrane because of SMMs concentration gradient across the membrane width [21–25].

Several SMMs preparation and application membrane modification have been reported [26–29]. Tang et al. [24] used the SMMs in the polymeric metrics for the first time and reported the migration phenomenon. Hamza et al. [9] observed that in comparison with the unmodified membranes, SMM surface-modified membranes were susceptible to less fouling in the treatment of cutting machine oil/water emulsion by ultrafiltration. Fang et al. [7] employed these kinds of surface-modified membranes to remove chloroform from water by pervaporation. Qtaishat et al. [19] have issued a patent reporting the effects of macromolecules properties in composition with polymeric membranes. One of the primitive works concerning with application of SMMs in membrane framework was reported by Khayet et al. [13]. They studied the surface modification of PVDF pervaporation membranes and reported the increase in the membrane hydrophobicity and operational performance. In another research, they reported on fluorinated asymmetric polyetherimide ultrafiltration membranes using SMMs [30,31]. In the similar work, Khayet et al. have performed a comparative study on SMM-modified membranes and commercial membranes in MD experiments [16].

Practically in all mentioned works, it was observed that membranes with SMM perform better than pristine membranes. Wherein the amount of SMM added to the polymeric cast solution is usually less than 5 wt%. Then in these studies, the reported surface properties relatively remained unchanged. In fact, the simultaneous optimization of doped SMM content and polymer concentration and their simultaneous influence on the final membrane characteristics are not investigated. Hence, various theoretical approaches have been developed to design the experiments of optimization in order to tackle these problems. Response surface methodology (RSM) is an assembly of mathematical and statistical methods that are useful for the modeling and analyzing this kind of problems. In this technique, the main objective is to optimize the response surface that is influenced by various process parameters. RSM also quantifies the relationship between the controllable input parameters and the obtained response surfaces [12].

Here the main part of work lays on the synthesis and characterization of SMM and empirical optimization of phase inversion parameters. For this aim, in the first step, the appropriate SMMs are synthesized and characterized using Fourier transform infrared (FTIR) and gel permeation chromatography (GPC). Then the PVDF/SMM-modified membranes are prepared at the various weight ratios using the phase inversion method. The resulted pristine and modified PVDF membranes are characterized to evaluate their surface hydrophobicity, morphology and porosity. Scanning electron microscope (SEM), energy-dispersive X-ray (EDX) spectroscopy and CA goniometry are used for this purpose. Finally, by collecting the experimental data, the RSM is employed to obtain the optimized values of preparation method. The ultimate PVDF/SMM membrane is synthesized using the
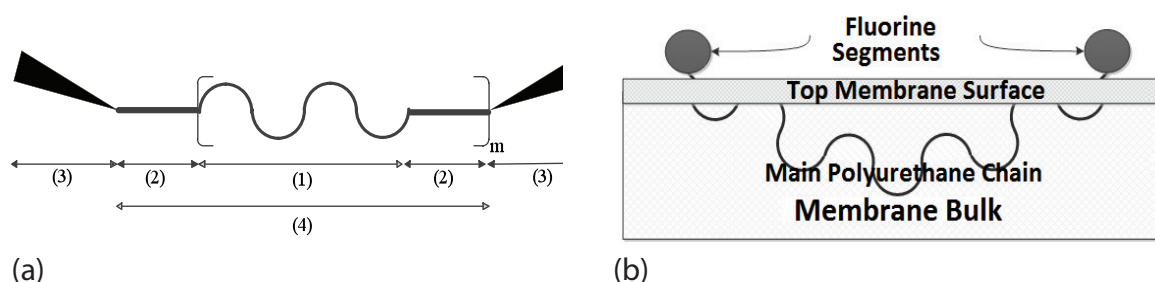

Fig. 1. (a) Structure of surface-modifying macromolecules: (1) polyol, (2) diisocyanate, (3) fluorine segment, and (4) main polyurethane chain and (b) structure of modified membrane with surface-modifying macromolecules.

optimized values, and its performance is evaluated experimentally in MD process in comparison with other ones.

2. Materials and methods

2.1. Materials

All chemicals used in this work together with their molecular structure and chemical abstract service (CAS) number are summarized in Table 1S from supplementary data. Employed materials were in synthetic grade and purchased from Sigma-Aldrich, Inc., St. Louis, MO, USA. The materials were used as received or were kept in appropriate conditions to be utilized.

2.2. SMM and membrane synthesis and characterization

The SMM was synthesized by two-step solution polymerization methods [13,14]. For this purpose, nitrogen flow is used inside a glove box to create an inert reaction environment. The first polymerization step is conducted for 3 h at 50°C in a solution of *N,N*-dimethylacetamide (DMAC) solvent with a pre-determined composition of reaction precursors of methylenebis(*p*-phenyl isocyanate) (MDI) and poly(propylene glycol) (PPG). MDI and PPG were reacted to form the required oligomers, i.e., pre-polymer, with hydrocarbon tails ended by hydroxyl groups. In the second polymerization step, which lasts for 24 h at 45°C–50°C, the pre-polymer is end-capped by the addition of 1*H*,1*H*,2*H*,2*H*-perfluoro-1-decanol (PFD), resulting in a solution of SMM in DMAC. Finally, the resulting polymer was precipitated with distilled water, and then washed in acetone/water 30 v/v% leaching solvent to eliminate unreacted monomers. The chemical structures of the prepared SMM and correspondent pre-polymer samples were investigated by a FTIR spectrometer (Brucker 3020, Germany). GPC (Agilent 1100-RID, USA) was used to measure the mean molecular weight of the membrane and weight distribution index.

The conventional phase inversion method was used to prepare pristine PVDF and modified PVDF/SMM membranes. The process is defined completely in supplementary data file. The morphology of the prepared membranes was studied using scanning electron microscope (SEM; Hitachi Model S 4100, Japan) equipped with the EDX (Oxford Instruments, USA). Water CAs of the membrane surfaces were measured by a contact angle goniometry (JYSP360, United Test, China). Membrane porosity (ε) was calculated using gravimetric method of supplementary data.

2.3. MD experiments

Direct contact membrane distillation (DCMD) experimental setup was used to test the permeation performance of the prepared optimum membrane for desalination. The detail description of the MD experimentation was represented in supplementary data.

2.4. Experimental design

RSM mathematical modeling was applied for analyzing the synthesis process of PVDF/SMM membranes.

As described earlier, there are many variables involved in the phase inversion technique that may affect the final membrane structure and MD performance. Therefore, it was necessary to select the parameters that had major effects on response [12]. For this purpose, the main parameters of PVDF/SMM synthesis such as PVDF concentration, SMM concentration and the evaporation of the casting process were selected regarding the results explained in supplementary data. The levels of the parameters were selected based on the experimentation results, and their independent and combined effects on the membrane surface properties, i.e., hydrophobicity, porosity and pore sizes, are evaluated through mathematical modeling. The mathematical model was developed for this system using Box–Behnken design and is described in the supplementary data.

3. Results and discussion

3.1. SMM characterization

The SMM agent synthesis process was similar to the previous works reported in the literature [13–15]. The structural composition of pre-polymer and SMM chemical structure were characterized by FTIR spectroscopy. Fig. 2(a) shows the obtained FTIR spectra of the SMM and pre-polymer samples. Pre-polymer spectrum shows the presence of unreacted isocyanate, which was confirmed by 2,082 cm^{-1} peak whereas SMM spectrum results from the addition of PFD. The diisocyanate (–N–C=O) absorption band at 2,250–2,275 cm^{-1} was not appeared in the spectrum of the resulting SMM, indicating that all unreacted isocyanate groups have been completely utilized by hydroxyl group of PFD. C–H aliphatic stretches bands (2,972 and 2,921 cm^{-1}) are also observed. There is a strong N–H stretching-vibration absorption peak at 3,280 cm^{-1}. The C=O stretching peak and N–H bending peak were observed at 1,720 and 1,538 cm^{-1}, respectively; the peak at 1,107 cm^{-1} was assigned to the stretching vibration of C–O–C; and the absorptions at 1,016 and 1,162 cm^{-1} were
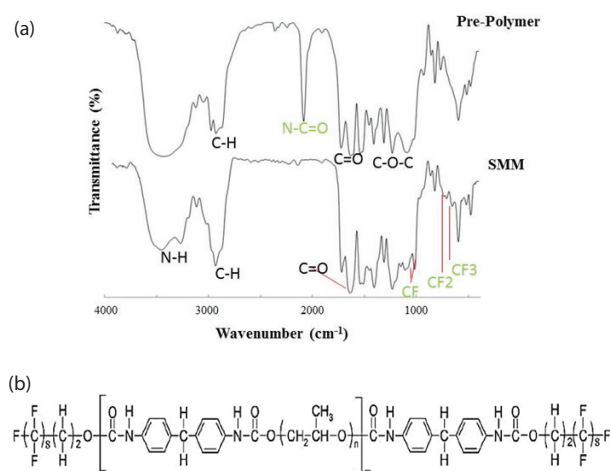

Fig. 2. (a) FTIR absorption spectra of the pre-polymer and SMM samples. The functional groups attributed to the absorption peaks are represented and (b) chemical structure of the synthesized surface-modifying macromolecule.

attributed to the stretching vibration of C–F. The absorption bands at 717 and 653 cm^{-1} are resulted from the stretching vibration of CF_3 and deformation vibration of CF_2, respectively [14]. The chemical structure of the synthesized SMM is shown in Fig. 2(b).

FTIR analyses confirm the formation of desired SMMs through the applied synthesize route. The average molecular weight of the SMM was measured by using GPC. The values of M_w, M_n and water CA for the synthesized SMM are given in Table 1. According to the structure of SMM presented in Fig. 2(b), the repetition number of propylene glycol units (n) equals to 7 and was calculated from the average M_w of PPG. In addition, repetition number of urethane units (m) equals 86.44 and was calculated from average M_w of SMM.

3.2. Effects of independent variables on responses

3.2.1. Effect of the PVDF concentration

Fig. 3(a) represents the influence of PVDF concentration on the membrane surface morphology and CA. The results of ANOVA (Table 4S from supplementary data) indicate that the PVDF concentration (x_1) has insignificant effect on the

Table 1
SMM characterization results: water contact angle (CA_w), mean molecular weight (M_w) and the mass number weight (M_n)

SMM	MDI:PPG:PFD
CA_w (°)	130
M_w (10^4 g/mol)	5.9547
M_n (10^4 g/mol)	3.8627

surface CA (p value = 0.4961 > 0.05). It was observed from Fig. 3(b) that increase in the PVDF concentration caused a very small decrease of the surface CA. It means that surface hydrophobicity is less affected by PVDF concentration. The explanation for this observation is that by rising of the PVDF concentration in the casting solution, viscosity of the polymer solution will be increased. Increase in the viscosity slowed down the SMM migration toward the top surface of membrane. As a result, surface CA is expected to be decreased. Suk et al. and Khayet et al. reported the similar result, respectively, for PES and PEI [22,13].

In addition, ANOVA results (Table 4S) illustrate that PVDF concentration (p value = 0.0006 < 0.05) has significant influence on the mean surface pore size of the membrane. By increasing the PVDF concentration, dope solution viscosity increased and packed structure (sponge-type structure) was formed. As a result, surface pore size and porosity was decreased by PVDF concentration (Figs. 3(c) and (d)). Tomaszewska [27] and Ortiz de Zárate et al. [32] reported the similar result for PVDF. They found that both the pore size and porosity increased with decrease of the PVDF concentration in the polymer casting solution.

3.2.2. Effect of SMM concentration

The obtained p value of 0.0001 < 0.05 for SMM concentration (x_2) indicates that this variable has significant influences on the surface CA responses (Table 4S). Fig. 4(b) shows the trend of CA variation with SMM concentration. As shown, increase in the SMM concentration intensifies the surface CAs. This could be explained as increasing the SMM concentration in the casting solution enhances the fluorine content of the top membrane surface due to which the surface CA must be increased [29].
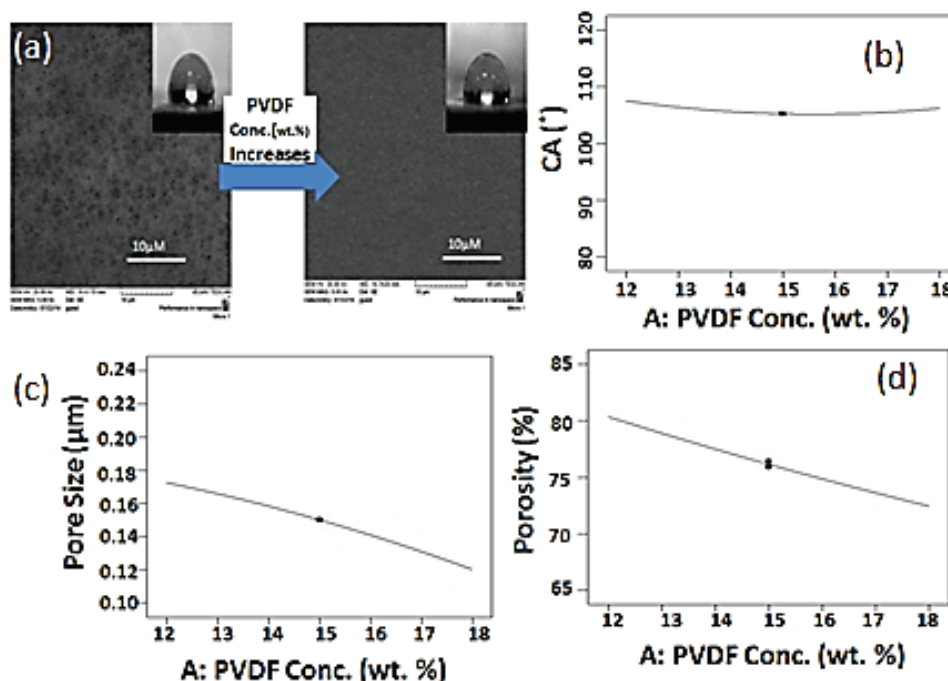

Fig. 3. (a) Surface morphology and water contact angle variation with PVDF concentration. The curves showing the effects of PVDF concentration on: (b) surface contact angle, (c) mean surface pore size and (d) overall porosity.
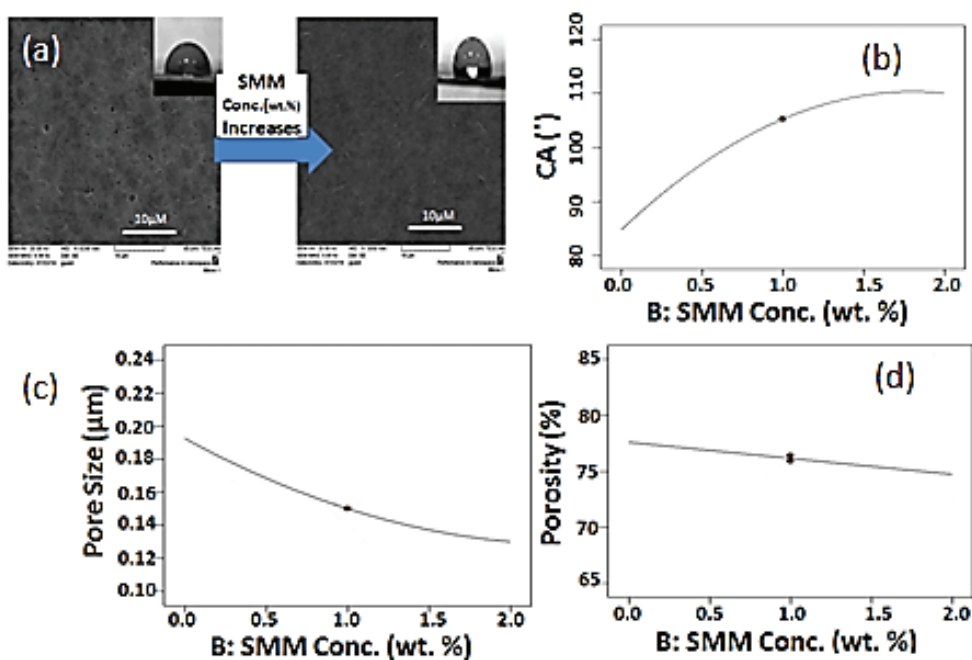
Fig. 4. (a) SEM and CA micrographs indicate the influence of SMM addition. The curves showing the effects of SMM concentration on: (b) surface contact angle, (c) mean surface pore size and (d) overall porosity.

Similar results were observed when blending SMM with other base polymers in phase inversion method [14,17].

The observed downward concavity in Fig. 4(b) is because of both negative coefficient of square of SMM concentration (x_2^2) (represented in supplementary data in Eq. (6)) and the significant influence of this parameter on response (p value = 0.0050 < 0.05). As described before, a small amount of SMM needs to saturate a membrane surface. Then at high SMM concentrations, CA does not increase further. Khayet and Matsuura [16] observed that saturation of the PVDF membrane surface could be reached at about 2 wt % of the SMM in the PVDF casting solution. Pham et al. [33] also reported that an SMM concentration of 0.5 wt% was a significant amount to saturate the PES surface.

The significant effect of the SMM concentration on the membrane surface hydrophobicity and pore size is visualized in Fig. 4(a). In addition, ANOVA results reported the SMM concentration (p value = 0.0003 < 0.05) has significant influence on the mean surface pore size. It was observed from Fig. 4(c) that increase in the SMM concentration results in diminishing of the mean surface pore size. In fact, by increasing the SMM concentration in the casting solution, it enriches on the membrane surface because of great tendency of migration to top of membrane. Therefore, the structure of top surface becomes denser, and as a result, the pore size will decrease. Prince et al. [18] and Khayet and Matsuura [14] reported the similar result, respectively, for PVDF and PEI.

Fig. 4(d) indicates that increase in the SMM concentration reduces the overall porosity of the membrane. This trend is due to viscosity of the casting solution as well as the thickening of the top sponge layer that decrease the porosity. However, by increasing the polymer content in the casting solution, the pore size, porosity and permeability gradually decrease.

3.2.3. Effect of solvent evaporation time

Regarding ANOVA results of Table 4S, solvent evaporation time (x_3) (p value = 0.0150 < 0.05) has considerable influence on the surface CA. Figs. 5(a) and (b) show the effect of solvent evaporation time on the surface CA. As can be seen, increase in solvent evaporation time prompts the increase of surface CA. As described, during the solvent evaporation time, the SMM molecules migrate to the membrane surface in order to minimize the surface free energy of the PVDF/SMM system. As a result, the surface CA will be increased by increasing the solvent evaporation time. Suk et al. [21–23] observed similar behavior for casting evaporation time. Khulbe et al. [17] found that the exposure time to the air is one of the major parameters for migration of SMM to the outer membrane surface and hydrophobicity improvement. Khayet [15] reported the similar result for SMM-modified PVDF membrane but it was found that by increasing the solvent evaporation time, the CA of the unmodified PVDF membranes did not change significantly. The increase in the CA suggests that the surface of the modified PVDF membrane becomes more hydrophobic.

Figs. 5(c) and (d) show surface mean pore size and porosity reductions by increasing the solvent evaporation time. As the solvent evaporation time is increased in modified membranes, the SMM components on the top membrane surface will be enriched due to their migration toward the membrane surface. However, for the pristine membrane, polymer concentration in the top cast film will be increased. Consequently, a denser structure is formed in the membrane's skin layer in both cases. Pore size and overall porosity of both types of membrane will be decreased.

Feng et al. [8] observed that both pore size and porosity of the PVDF–HFE membrane decreased with increasing solvent evaporation time. Khayet et al. [13] observed that the mean
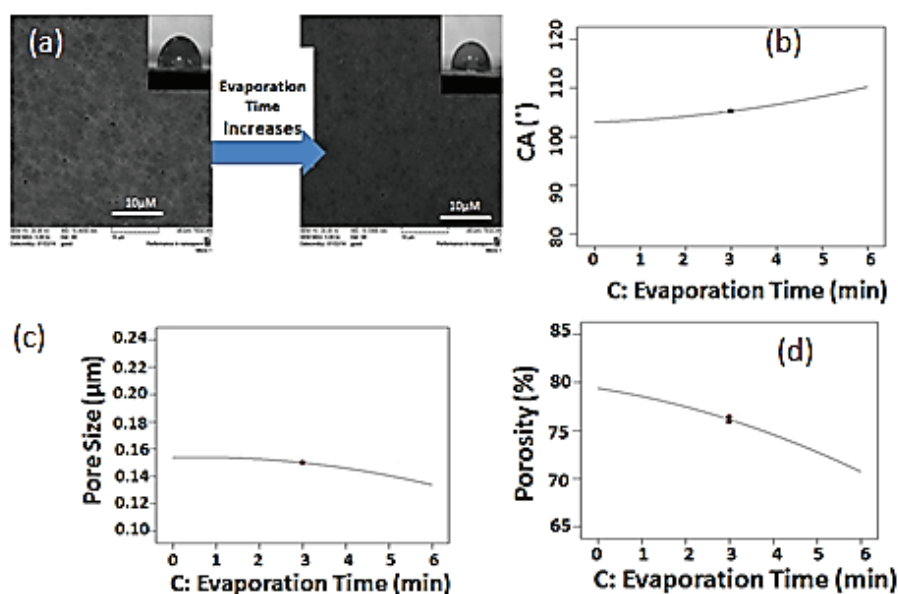
Fig. 5. The curves showing the effects of solvent evaporation time on: (b) surface contact angle, (c) mean surface pore size and (d) overall porosity.

pore size of the unmodified PEI membrane was larger than those of the SMM-modified PEI membranes and decreased with the increase in the solvent evaporation time.

Table 4S illustrates that the solvent evaporation time (p value = 0.0003 < 0.05) has significant influence on the membrane overall porosity.

Fig. 5(d) shows overall porosity decreased by increasing the solvent evaporation time. As mentioned earlier, by increasing the solvent evaporation time, SMM concentration for modified membranes and PVDF concentration for unmodified membranes will be increased in the top cast film layer. As a consequence, a denser structure is formed, and overall porosity of the membrane will be decreased.

Qtaishat et al. [19] reported the similar result for SMM-modified PEI membranes. They found that the size and number of macrovoids decreased with an increase in the evaporation time and the sponge-like structure between macrovoids became thicker. He found that both the pore size and effective porosity were higher when membranes prepared without solvent evaporation time [19,20].

3.3. The interaction between the variables

The three-dimensional (3D) response surface plots are the graphical representations of the regression equation. These plots were presented in Figs. 6 and 7. Figs. 6(a) and (b) are illustrating the surface CA changes with SMM and PVDF concentrations; Figs. 6(d) and (f) are for mean surface pore size; and Figs. 6(c) and (e) are for overall porosity. These types of plots showed effects of two factors on the response at a time. In all the presented figures, the other factor was kept at zero level.

According to Figs. 6(d) and (f), the mean surface pore size decreased with increasing the concentrations of both the SMM and PVDF in the casting solution and also increase in the solvent evaporation time.

The minimum value mean of surface pore size is obtained when the membrane prepared with high concentration of both the PVDF and SMM. In addition, applying long solvent evaporation time results in similar observation. As could be seen in Figs. 6(c) and (e), decrease in the PVDF concentration, SMM concentration and solvent evaporation time caused to increase the membrane overall porosity. The overall porosity of prepared membrane is maximum value when both the PVDF and SMM concentration were very low and membrane prepared without any solvent evaporation time.

The combined effects of evaporation time and SMM concentration on membrane properties are exhibited 3D response surface plots of Fig. 7. As can be seen in Fig. 7(a), an increase in surface CA was observed with increase in both the SMM concentration and solvent evaporation time and decrease in PVDF concentration. This type of synchronize variation result in increase of the mean pore size of the membrane (Fig. 7(b)). However, as could be seen in Fig. 7(c), it does not effectively change the membrane porosity.

In fact, the results indicate that maximum CA was obtained using very low PVDF concentration, using SMM concentration higher than 1.5 wt% and applying the maximum solvent evaporation time.

3.4. Validation of the model

By using the modeling results, the optimum values of the variables were determined to obtain maximum CA, maximum porosity and minimum pore size. Achieving this characteristics is to inhibit pore wetting, and obtain high permeate flux. High surface hydrophobicity and low pore size result in high liquid entry pressure (LEP) values that inhibit pore-wetting phenomena. These optimal values were obtained as 12 wt% for PVDF concentration, 1.75 wt% for SMM concentration and 0.46 min for solvent evaporation time. The corresponding
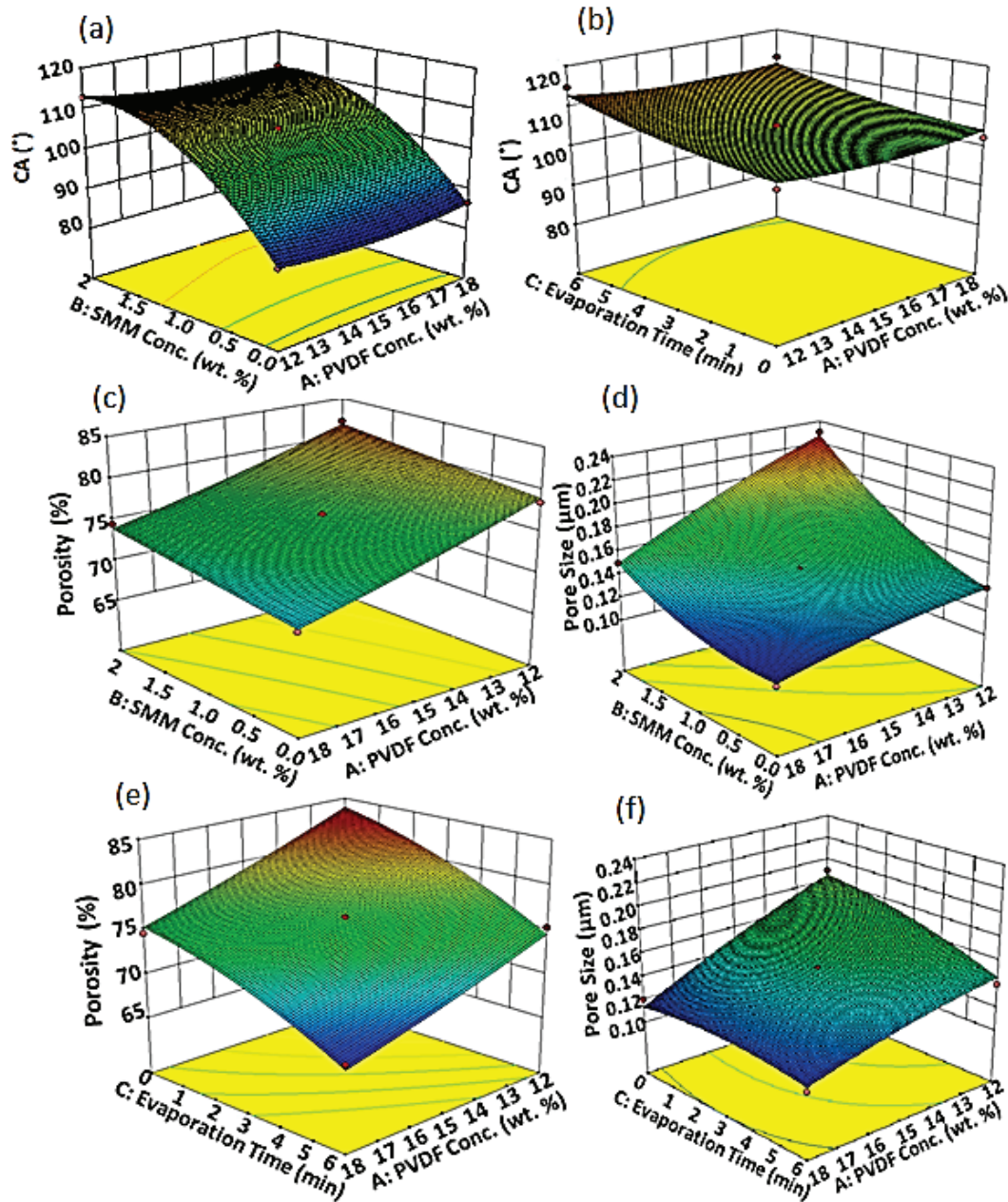
Fig. 6. 3D response surface plots of the interaction between the varriables: the effect of PVDF concentration in combination with: (a) SMM concentration on contact angle, (b) solvent evaporation time on contact angle, (c) SMM concentration on porosity, (d) SMM concentration on pore size, (e) solvent evaporation time on porosity and (f) solvent evaporation time on pore size.

responses were: CA = 109.4°, pore size = 0.152 μm and porosity = 83.11. In order to validate the accuracy of the model equations, a verification experiment was carried out under the optimal conditions. The characterization results for the optimal membrane and pristine one are summarized in Table 2. As shown, the mean values of 108°, 80% and 0.145 μm are measured, respectively, for water CA, porosity and pore size. In comparison with obtained experimental values, the calculated response values were in close agreement with the validation of employed Box–Behnken model.

3.5. Morphological study

The weight and atomic percentages of existing elements on the optimum membrane cross section is determined using EDX image analysis (Fig. 8). As illustrated, the presence of N and O is just due to the SMM structure, but other elements (C and F) are existing in both the SMM and PVDF. In addition, Fig. 8 indicates the EDX spectrum of the optimum membrane cross section. The spectrum confirms the abundance of fluorine on the membrane composition.
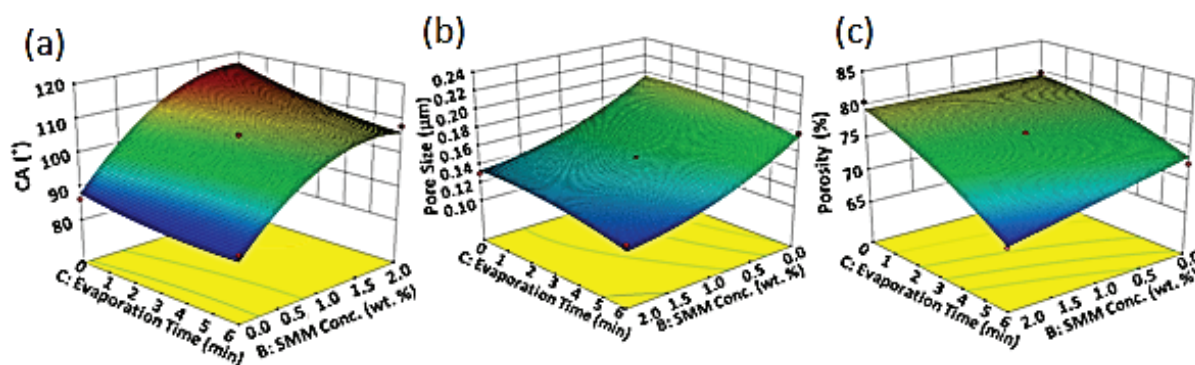
Fig. 7. 3D response surface plots for the effect of SMM concentration in combination with evaporation time on: (a) contact angle, (b) pore size and (c) porosity.

Table 2
Comparative characteristics of PVDF and optimal PVDF/SMM membranes

Membrane type	Contact angle		Porosity (%)	Mean pore size (μm)
	Top surface (°)	Bottom surface (°)		
PVDF (pristine)	86.5	84.0	84.6	0.240
PVDF/SMM (optimal)	108.1	86.3	80.0	0.145

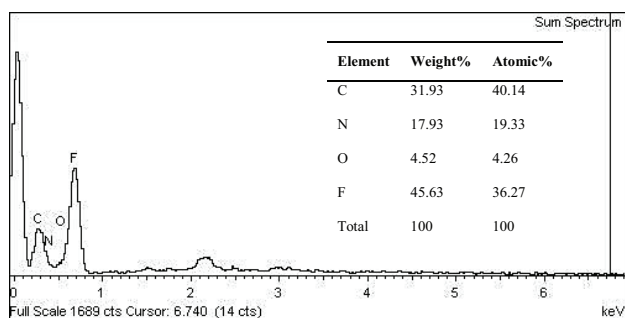| Element	Weight%	Atomic%
C	31.93	40.14
N	17.93	19.33
O	4.52	4.26
F	45.63	36.27
Total	100	100

Fig. 8. EDX spectrum of the optimum membrane cross section. The complete summary of the EDX analysis results are revealed.
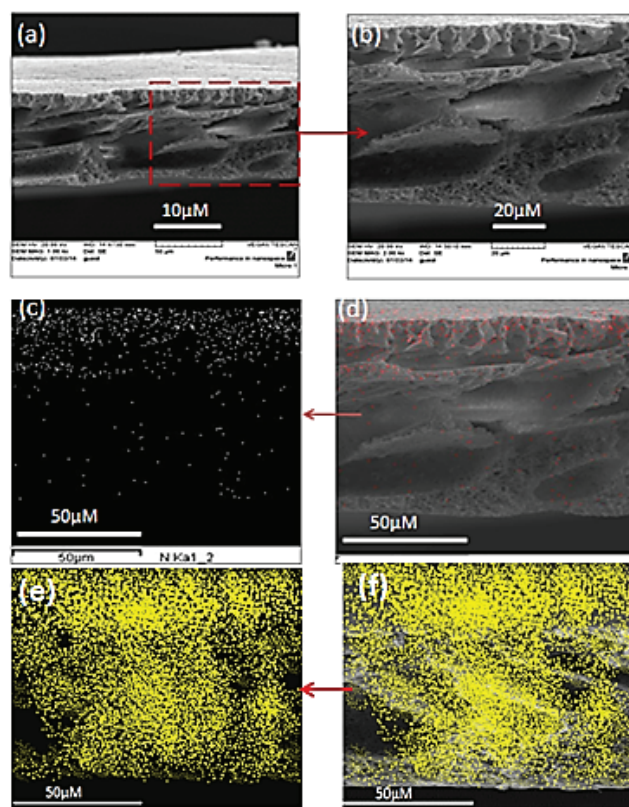

Fig. 9. (a) The SEM image of the membrane cross section, (b) magnified SEM image, (c) EDX spectra of nitrogen throughout the membrane cross section, (d) nitrogen image mapping on the membrane cross section, (e) EDX spectra of fluorine throughout the membrane cross section and (f) fluorine elemental mapping on the membrane cross section.

The SEM images of the membrane cross section and top surface are shown in Figs. 9(a) and (b). As could be observed, the membrane shows an asymmetric structure with a sponge top layer and macrovoids underneath. The formation of the top layer sponge-like structure is due to the slow polymer/ SMM coagulation during solvent evaporation time and SMM migration. During the solvent evaporation stage, partial solidification of the polymer film and SMM segregation toward the polymer/air interface occurs, forming a thin skin layer of solid SMM/polymer due to the loss of solvent.

The porous thin layer that forms during solvent evaporation time becomes the top skin layer governing the MD

performance of the membrane, while the porous structure having macrovoids that forms during the solvent-water exchange becomes the porous sub-layer, providing the mechanical strength to the membrane. According to Table 1, fluorine exists in both PVDF and SMM polymers, while nitrogen only exists in the SMM polymer; as a result,

SMM migration to the top membrane surface is determined by nitrogen distribution analysis. However, the fluorine elemental mapping is performed, and the results are indicated in Figs. 9(e) and (f).

Figs. 9(a) and (b) represent the SEM cross-sectional morphology of the optimum membrane together with the EDX spectra of nitrogen (EDX elemental mapping) at Figs. 9(c) and (d). The migration of SMM can be confirmed by higher concentration of nitrogen on the top surface of modified membranes compared with the unmodified membranes, rendering its hydrophobicity and confirming the results of the water CA tests [10,30]. Nitrogen elemental mapping identifies the presence and population profile of the SMMs across the membrane cross section. It is obvious from Fig. 9(d) that the concentration of SMMs on the membrane surface is higher than the membrane bulk and down side. The similar trend was obtained in the case of fluorine elemental distribution along the membrane top-surface in comparison with down-surface (Fig. 9(f)).

3.6. MD performance of optimal membrane

The optimum membrane was tested for desalination by DCMD and air gap membrane distillation (AGMD) processes. The details of relevant experiments are presented in supplementary data. Experimental results show that DCMD method performs better than AGMD. Then the DCMD tests are evaluated for modified membrane using the flow diagram represented in Fig. 10. The permeate flux of the membrane in two different NaCl concentrations in feed solution (0.5 and 1 mol/L) and three different feed temperatures (68°C, 75°C and 83°C) in DCMD process are shown in
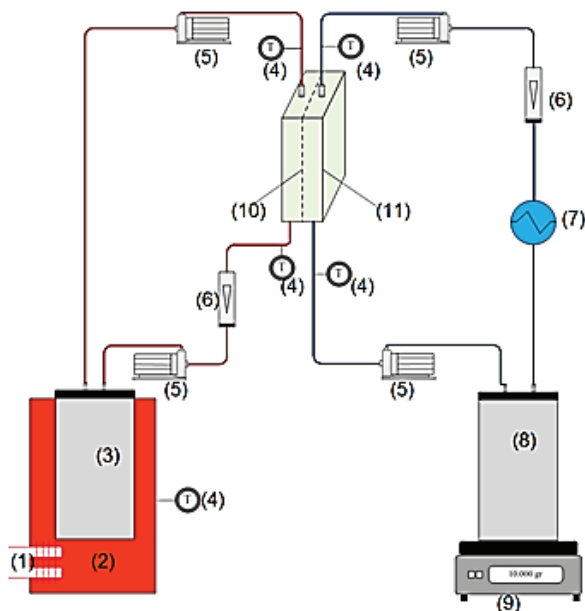

Fig. 10. Schematic of DCMD experimental setup.
Note: (1) – Water heater, (2) – hot water bath, (3) – feed tank, (4) – thermocouple, (5) – peristaltic pump, (6) – flow meter, (7) – condenser, (8) – permeate tank, (9) – balance, (10) – membrane and (11) – DCMD module.

Figs. 11(a) and (b). It should be mentioned that the rejection factor of NaCl during all the DCMD was 99.99%.

As can be seen in Fig. 11(a), in DCMD process, the permeate flux increases with rising feed temperature. The exponential increase of the vapor pressure of the feed aqueous solution with temperature (i.e., Antoine equation), which enhances the driving force (i.e., vapor pressure difference) for both water and the volatile solutes present in the feed solution. The increases of the non-volatile solute concentration in the feed aqueous solution result in a reduction of the DCMD permeate flux. This behavior is attributed to the decrease of the water vapor pressure, the driving force, with the addition of non-volatile solute in water due to the decrease in water activity of the feed [30]. According to the obtained results, the higher fluxes of DCMD are obtained in NaCl concentration of 0.5 mol/L.

Finally, in order to compare the permeate flux and salt rejection of the optimum modified membrane with the unmodified membrane prepared at same preparation conditions but without the SMM (with 12 wt% of PVDF, 88 wt% of DMAC and solvent evaporation time of 0.46 min), both membranes were tested for desalination in the obtained MD conditions of higher flux (feed concentration of 0.5 mol/L and DCMD method).

As can be seen in Figs. 11(b) and (c), both permeate flux and salt rejection of the modified membrane was higher than the unmodified membrane. In unmodified membranes, low PVDF concentration leads to high porosity and large mean pore size (large voids) resulting in low LEP values as described earlier that result in reduction of selectivity. Low CA of unmodified membranes was because of the absence of SMM, which amplifies pore wetting and reduces salt rejection efficiency. Also, absence of SMM causes the unmodified membrane to be single layer, leading to an increase in heat loss and a decrease in mass transfer, decreasing the permeate flux.

The measurement of the water permeation flux (J_w) reveals that the MD permeation flux for the optimally modified PVDF/SMM membrane is 17.5 Kg/m²h at 83°C. While in the case of pristine PVDF membrane, this value is about 15.0 Kg/m²h at the same experiments. In addition, the salt rejection efficiency of the presented PVDF/SMM membrane is above 99.9% that is higher than 99.5% the neat membrane salt rejection percentage. To gain the better evaluation, the abstract comparison of the results was performed with other surface engineered membranes reported in the recent works [14–17]. The obtained values of the hydrophobicity, porosity and the salt rejection performance are higher than those reported in similar works. However, the permeate flux of the optimally engineered PVDF/SMM membrane lay in the same range.

4. Conclusions

SMMs was synthesized and characterized by FTIR spectrometry and GPC. The modified PVDF composite membranes were prepared using SMM through non-solvent-induced phase inversion process. RSM was used to obtain the optimal PVDF/SMM membrane preparation conditions. For this purpose, a mathematical model was developed using the empirical data of PVDF/SMM
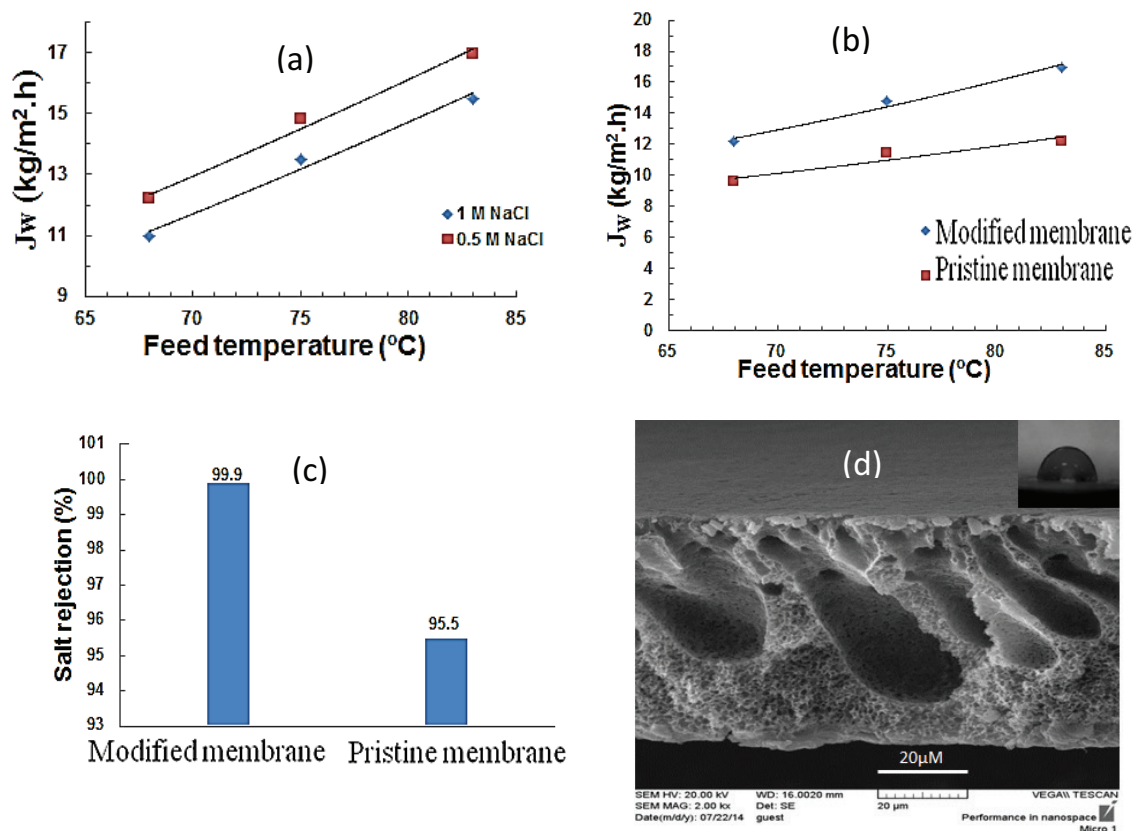
Fig. 11. (a) Effect of feed temperatures and NaCl concentrations on DCMD permeate flux; (b) variation of DCMD permeate flux as a function of feed temperature for modified and pristine PVDF membrane (feed salt concentration is 0.50 molar); (c) salt rejection efficiency for modifies and pristine PVDF membranes, and (d) cross section image of the pristine PVDF membrane with contact angle image.

synthesis experiments. The behavior of the independent variables was evaluated in the synthesis process, and their interactions on each other were analyzed. Optimization results were employed to prepare modified PVDF/SMM membrane. Results indicate that the presence of SMM converts the membrane to bilayer dual characteristics form, which leads to a decrease in heat loss and an increase in the mass transfer. The modified membranes reveal higher water CAs than those of unmodified ones. A DCMD permeate flux 17% higher than that of pristine membrane was obtained. The salt rejection factor was found to be higher than 99.9% for the optimally modified PVDF/SMM membrane.

References

[1] A.M. Alklaibi, N. Lior, Membrane-distillation desalination: status and potential, Desalination, 171 (2004) 111–131.

[2] R. Moradi, J. Karimi-sabet, M. Shariati-niassar, M.A. Koochaki, Preparation and characterization of polyvinylidene fluoride/graphene superhydrophobic fibrous films, Polymers, 7 (2015) 1444–1463.

[3] K.C. Chong, S. Lai, K.M. Lee, O.B. Seng, Desalination and water treatment characteristic and performance of polyvinylidene fluoride membranes blended with different additives in direct contact membrane distillation, Desal. Wat. Treat., 54 (2014) 3218–3226.

[4] E. Curcio, E. Drioli, Membrane distillation and related operations: a review, Sep. Purif. Rev., 34 (2005) 35–86.

[5] R. Moradi, J. Karimi-Sabetb, M. Shariaty-Niassara, Y. Amini, Air gap membrane distillation for enrichment of $H_2^{18}O$ isotopomers in natural water using poly(vinylidenefluoride) nanofibrous membrane, Chem. Eng. Process., 100 (2016) 26–36.

[6] M.S. El-Bourawi, Z. Ding, R. Ma, M. Khayet, A framework for better understanding membrane distillation separation process, J. Membr. Sci., 285 (2006) 4–29.

[7] Y. Fang, V.A. Pham, T. Matsuura, J.P. Santerre, R.M. Narbaitz, Effect of surface-modifying macromolecules and solvent evaporation time on the performance of polyethersulfone membranes for the separation of chloroform/water mixtures by pervaporation, J. Appl. Polym. Sci., 54 (1994) 1937–1943.

[8] C. Feng, B. Shi, G. Li, Y. Wu, Preliminary research on microporous membrane from F2.4 for membrane distillation, Sep. Purif. Technol., 39 (2004) 221–228.

[9] A.V. Hamza, V.A. Pham, T. Matsuura, J.P. Santerre, Development of membranes with low surface energy to reduce the fouling in ultrafiltration applications, J. Membr. Sci., 131 (1997) 217–227.

[10] J.Y. Ho, The effect of surface modifying macromolecules on the blood compatibility of polyethersulfone membrane intended for biomedical applications, MSc Dissertation, University of Toronto, 1997.

[11] J.Y. Ho, T. Matsuura, J.P. Santerre, The effect of fluorinated surface modifying macromolecules on the surface morphology of polyethersulfone membranes, J. Biomater. Sci. Polym. Ed., 11 (2000) 1085–1193.

[12] J. Karimi-Sabet, C. Ghotbi, F. Dorkoosh, Application of response surface methodology for optimization of paracetamol particles formation by RESS method, J. Nanomater., 12 (2012) 15–30.

[13] M. Khayet, D.E. Suk, R.M. Narbaitz, J.P. Santerre, T. Matsuura, Study on surface modification by surface-modifying macromolecules and its applications in membrane-separation processes, J. Appl. Polym. Sci., 89 (2003) 2902–2916.

[14] M. Khayet, T. Matsuura, Progress in membrane surface modification by surface modifying macromolecules using polyethersulfone, polyetherimide and polyvinylidene fluoride base polymers: applications in the separation processes ultrafiltration and pervaporation, Fluid/Part. Sep. J., 15 (2003) 9–21.

[15] M. Khayet, Membrane surface modification and characterization by X-ray photoelectron spectroscopy, atomic force microscopy and contact angle measurements, Appl. Surf. Sci., 238 (2004) 269–272.

[16] M. Khayet, T. Matsuura, Preparation and characterization of polyvinylidene fluoride membranes for membrane distillation, Ind. Eng. Chem. Res., 40 (2001) 5710–5718.

[17] K.C. Khulbe, C.Y. Feng, T. Matsuura, D.C. Mosqueda-Jimenez, M. Rafat, D. Kingston, R.M. Narbaitz, M. Khayet, Characterization of surface modified hollow fiber polyethersulfone membranes prepared at different air gaps, J. Appl. Polym. Sci., 104 (2007) 710–721.

[18] J.A. Prince, D. Rana, G. Singh, T. Matsuura, T. Jun Kai, T.S. Shanmugasundaram, Effect of hydrophobic surface modifying macromolecules on differently produced PVDF membranes for direct contact membrane distillation, Chem. Eng. J., 242 (2014) 387–396.

[19] M. Qtaishat, M. Khayet, T. Matsuura, Novel porous composite hydrophobic/hydrophilic polysulfone membranes for desalination by direct contact membrane distillation, J. Membr. Sci., 341 (2009) 756–767.

[20] M. Qtaishat, D. Rana, M. Khayet, T. Matsuura, Preparation and characterization of novel hydrophobic/hydrophilic polyetherimide composite membranes for desalination by direct contact membrane distillation, J. Membr. Sci., 327 (2009) 245–251.

[21] D.E. Suk, G. Pleizier, Y. Deslandes, T. Matsuura, Effects of surface modifying macromolecule (SMM) on the properties of polyethersulfone membranes, Desalination, 149 (2002) 303–307.

[22] D.E. Suk, T. Matsuura, H.B. Park, Y.M. Lee, Synthesis of a new type of surface modifying macromolecules (nSMM) and characterization and testing of nSMM blended membranes for membrane distillation, J. Membr. Sci., 277 (2006) 177–185.

[23] D.E. Suk, G. Chowdhury, T. Matsuura, R.M. Narbaitz, P. Santerre, G. Pleizier, Y. Deslandes, Study on the kinetics of surface migration of surface modifying macromolecules in membrane preparation, Macromolecules, 35 (2002) 3017–3021.

[24] Y.W. Tang, J.P. Santerre, R.S. Labow, D.G. Taylor, Use of surface-modifying macromolecules to enhance the biostability of segmented polyurethanes, J. Biomed. Mater. Res., 35 (1997) 371–381.

[25] Y.W. Tang, J.P. Santerre, R.S. Labow, D.G. Taylor, Synthesis of surface-modifying macromolecules for use in segmented polyurethanes, J. Appl. Polym. Sci., 62 (1996) 1133–1145.

[26] Y.W. Tang, J.P. Santerre, R.S. Labow, D.G. Taylor, Application of macromolecular additives to reduce the hydrolytic degradation of polyurethanes by lysosomal enzymes, Biomaterials, 18 (1997) 37–45.

[27] M. Tomaszewska, Preparation and properties of flat-sheet membranes from polyvinylidene fluoride for membrane distillation, Desalination, 104 (1996) 1–11.

[28] R.S. Ward, K.A. White, C.B. Hu, Use of Surface-Modifying Additives in the Development of a New Biomedical Polyurethaneurea, H. Planck, G. Egbers, I. Syré, Eds., Polyurethanes in Biomedical Engineering, Elsevier, Amsterdam, 1984.

[29] M. Shin, Y.H. Lee, M.M. Rahman, H. Kim, Synthesis and properties of waterborne fluorinated polyurethane-acrylate using a solvent/emulsifier-free method, Polymer, 54 (2013) 4873–4882.

[30] M. Khayet, T. Matsuura, Membrane Distillation: Principles and Applications, Elsevier, 2011.

[31] M. Khayet, C.Y. Feng, T. Matsuura, Morphological study of fluorinated asymmetric polyetherimide ultrafiltration membranes by surface modifying macromolecules, J. Membr. Sci., 213 (2003) 159–180.

[32] J.M. Ortiz de Zárate, L. Pẽna, J.I. Mengual, Characterization of membrane distillation membranes prepared by phase inversion, Desalination, 100 (1995) 139–148.

[33] V.A. Pham, J.P. Santerre, T. Matsuura, R.M. Narbaitz, Application of surface modifying macromolecules in polyethersulfone membranes: influence on PES surface chemistry and physical properties, J. Appl. Polym. Sci., 73 (1999) 1363–1378.

Supplementary data

1. Membrane distillation configurations

Membrane distillation (MD) is a non-isothermal membrane operation in which the driving force is the partial vapor pressure difference across the porous and hydrophobic membrane. MD has potential application for desalination purposes and is successfully employed in other fields such as waste treatment and food industry. One of the main advantages of MD is to operate in the moderate temperatures and pressures. There is a temperature difference between two sides of the membrane make the permeate flux through the hydrophobic membrane. Regarding the low operation temperatures in such a process, various cheap energy sources, like solar energy and waste heat, could be used. This is a key point in the application of expensive separation processes such as desalination. In this process, diffused vapor molecules are transformed into cold product using four different methods: (a) a cold liquid in direct contact with the membrane (DCMD), (b) a cold surface separated from the membrane by an air gap (AGMD), (c) a cold sweeping gas (SGMD), or (d) a vacuum (VMD) (Fig. 1S).

2. Experimental

2.1. Materials

Table 1S summarizes the materials used together with molecular structure and their chemical abstract service (CAS) number.

2.2. SMM and membrane synthesis and characterization

SMM was synthesized using conventional polyurethane chemistry. Methylenebis(*p*-phenyl isocyanate) (MDI) was used as the backbone of polymeric chain and was reacted with poly(propylene glycol) (PPG) as a polyalcohol. The produced oligomers end-caped appropriate fluoroalcohol of 1*H*,1*H*,2*H*,2*H*-Perfluoro-1-decanol (PFD). Prepared samples were dried in an oven at 50°C for 5 d. The molar mixing ratio of the chemicals MDI:PPG:PFD was 3:2:2.

For the synthesized SMM, the number (M_n) and weight (M_w) average molecular weights, and the index of the molecular weight distribution (M_w/M_n) were measured by gel permeation chromatography (GPC; Agilent 1100-RID, USA) at 30°C. SMM was dissolved in tetrahydrofuran and filtered with a 0.45-µm filter to remove high molecular weight components. Polystyrene was used as the calibration standard.

The obtained functional groups of the obtained pre-polymer and SMM were investigated by a Fourier transform infrared (FTIR) spectrometer (Brucker 3020, Germany) in the range 4,000–400 cm⁻¹. At the end of each step, 1 ml of each solution was placed under vacuum to remove the solvent until they became viscose. Finally, two drops of each solution were dropped onto the KBr discs.

In order to measure the contact angle of SMM polymer, a solution with 12 wt% of SMM in DMAC was prepared and cast on a glass plate to a thickness of 0.3 mm. The cast film together with the glass plate was placed in a vacuum drying
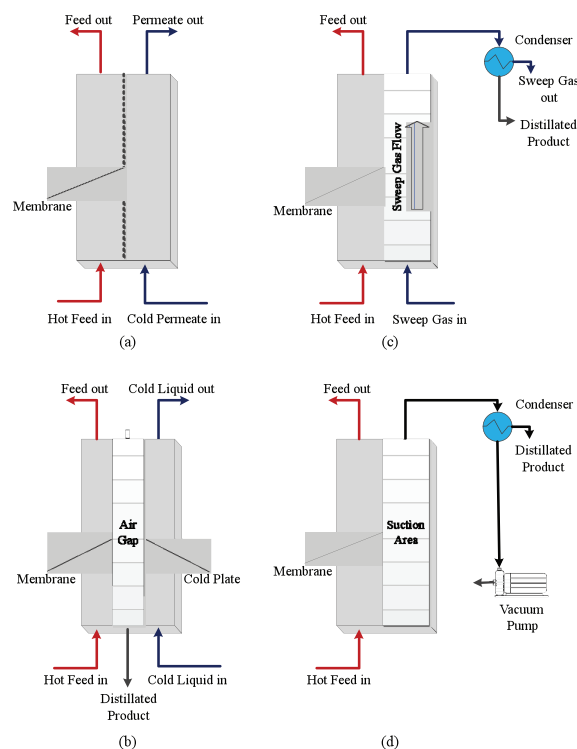

Fig. 1S. Membrane distillation configuration: (a) DCMD; (b) AGMD; (c) SGMD and (d) VMD.
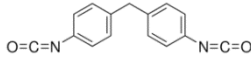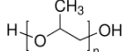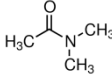
oven maintained at 60°C until the solvent was completely evaporated. For lowering the effects of pores and surface roughness, the dense film of SMM was prepared, and the water contact angle was measured by a contact angle goniometer (JYSP360, United Test, China).

Flat-sheet membranes were prepared by the phase-inversion method. First, PVDF was dissolved in DMAC (12.0 wt%) and stirred at 50°C for about 12 h to ensure the complete dissolution of the polymer. Then the prepared solution was used to prepare the pristine PVDF membranes. For the preparation of PVDF/SMM membranes, different concentrations of SMM were dissolved into the prepared PVDF casting solutions, and the solutions were allowed to stir at ambient temperature for at least 8 h. The mixture was then degassed over night at room temperature. The polymer solutions were cast on a smooth glass plate to a thickness of 0.25 mm using a motorized film applicator with a casting speed of 1 m/min. The solvent was then evaporated at room temperature for a predetermined period (0, 3 and 6 min) before the cast films were immersed together with the glass plates for 1 d in distilled water at 22°C.

During coagulation, the membrane spontaneously peeled off the glass substrate. The membranes were firstly immersed in an aqueous ethanol solution 33 wt% for 1 h, then in an aqueous ethanol solution 66 wt% and finally in pure ethanol for 2 h. Furthermore, the membranes were dried at room temperature for 1 d to complete the drying process.

The cross section and top surface of the membranes were analyzed by the scanning electron microscope (SEM; Hitachi Model S 4100, Japan) equipped with the energy-dispersive X-ray spectrometer (EDX; Oxford Instruments, USA). First,

Table 1S
Materials used for preparation of modified PVDF membranes

Material description	CAS number	Molecular structure/liner formula	Source
4,4'-Methylenebis(phenyl isocyanate) (MDI, 98%)	101-68-8	$O=C=N$ —⟨⟩—CH_2—⟨⟩—$N=C=O$ $CH_2(C_6H_4NCO)_2$	Sigma-Aldrich, Inc., St. Louis, MO, USA
1H,1H,2H,2H-Perfluoro-1-decanol (PFD, M_w = 464.12, 97%)	678-39-7	$CF_3(CF_2)_7CH_2CH_2OH$	Sigma-Aldrich, Inc., St. Louis, MO, USA
Poly(vinylidene fluoride) (average M_w ~530,000, pellets)	24937-79-9	$(CH_2CF_2)_n$	Sigma-Aldrich, Inc., St. Louis, MO, USA
Sodium chloride (NaCl)	7647-14-5	NaCl	Sigma-Aldrich, Inc., St. Louis, MO, USA
Tetrahydrofuran (THF, HPLC grade, 99.9%)	109-99-9	C_4H_8O	Sigma-Aldrich, Inc., St. Louis, MO, USA
Poly(propylene glycol) (PPG, M_n = 425)	25322-69-4	$H[OCH(CH_3)CH_2]_nOH$	Sigma-Aldrich, Inc., St. Louis, MO, USA
N,N-Dimethylacetamide (DMAC, anhydrous, 99.8%)	127-19-5	$CH_3CON(CH_3)_2$	Merck, Inc., Massachusetts 01821, USA

the membrane sample was fractured in liquid nitrogen and then sputter-coated with a thin layer of gold.

In order to find out the effect of SMM on the membrane properties, the cross section was analyzed by EDX to determine the nitrogen, fluorine, carbon and oxygen content throughout the membrane cross section using the software INCA (Oxford Instruments, USA). The distribution of nitrogen elements over membrane cross section can be viewed using element maps. Element mapping utilizes the X-ray signal from a specified energy range in order to show the elemental distribution. The mean pore size of the top membrane surfaces (SEM pictures) was measured by Image Tool picture analysis software (UTHSCSA).

Contact angles of deionized water on the top and bottom surfaces of the membranes were measured by a contact angle goniometry (JYSP360, United Test, China) at room temperature. In this study, the reported contact angle was the average of three different measurements.

In order to find the overall porosities, the membranes were placed in isopropanol for 1 d until it is fully penetrated; then the membrane porosities were measured by determining their swelling in isopropanol using the following expression

$$\varepsilon = \frac{W_2 - W_1}{S.d.\rho} \tag{1}$$

where ε is membrane overall porosity, W_1 and W_2 are weights of the membranes in the dry and wet states, respectively;

S and d represent the area and the average thickness of the membrane in the wet state, respectively, and ρ stands for the density of isopropanol at room temperature.

2.3. MD experiments

DCMD and AGMD experimental setup was used to test the permeation performance of the prepared optimum membrane for desalination. Both the feed and permeate circulated through the membrane module by means of a double-head peristaltic pump (Watson Marlow, 323). The temperature of the feed solution was controlled by a heating thermostat (501A, Shanghai Experimental Instrument Co., Ltd., China) and that of the distillate water was controlled by a cooling thermostat (DTY-10A, Beijing Detianyou Technology Development Co., Ltd., China). The inlet temperature of the feed solution into the module was maintained at three different temperature (68°C, 75°C and 83°C) for two different feed concentration (0.5 and 1 mol/L) for both DCMD and AGMD. The effective membrane area of both DCMD and AGMD systems was 0.49 × 10^{-3} m². Fig. 10 of the main text shows the setup used to conduct the DCMD experiments. In the DCMD configuration, hot feed solution was brought into contact with the top layer of the membrane, and the cold permeate solution is in contact with the bottom layer of the membrane. The temperature of the cold distillate water in DCMD was kept at 15°C. Fig. 2S shows schematic of AGMD experimental setup. In the AGMD configuration, evaporated water molecules at the liquid/membrane interface cross the membrane

pores and the air gap chamber to finally condense over the cooling stainless steel metallic plate. The temperature of the cold plat in AGMD was kept at 15°C.

It should be mentioned that each of the DCMD and AGMD experimental tests was carried out for 2 h. At the end, the MD conditions for reaching higher flux were found. Finally, the optimum modified membrane and the unmodified membrane at same preparation condition but without SMM additive were used in MD experiment under the higher MD flux conditions to see the effect of SMM addition on permeate flux and salt rejection. Permeation flux of the membranes was calculated by the following equation:

$$J = \frac{W}{A \cdot t} \tag{2}$$

where J is the pure water flux (Kg/(m²·h)); W is the permeation mass of water (Kg); A is the effective membrane areas (m²); and t is the sampling time (h). The solute rejection (R) of membrane was obtained from the following equation:

$$R = \left(1 - \frac{c_1}{c_2}\right) \times 100\% \tag{3}$$

where c_1 and c_2 are the solute concentration of permeate and feed solution, respectively, that was measured by water quality meter (Model 900, Bante Co., China).

2.4. Range of PVDF concentration

When the polymer content of the precursor solution is less than a threshold value (e.g., 10 wt% for PVDF), large holes appear within the membrane that strongly will effect on the membrane performance (selectivity).

On the other hand, by increasing the base polymer concentration in the PVDF/SMM solution, viscosity of the polymer solution will be increased, which slowed down SMM migration to the top membrane surface. It was observed that the membrane prepared by 12 wt% PVDF (without SMM and considering the evaporation time effects) is fragile with poor surface features. Where in the case of 20 wt% PVDF, at the same synthesize condition, the obtained membrane surface was smooth with low porosity. By adding 1.0 wt% SMM into this membrane due to weak SMM migration toward the surface, the thick skin layer with small pores (~90 nm) formed. The SEM and image analyzing results illustrated in Fig. 3S confirm this observation.

2.5. Range of SMM concentration

In the preparation of modified membranes to avoid altering the bulk properties and also to create a very thin hydrophobic layer on top of the membrane, less than 4 wt% SMM usually was used. In addition, it was reported that the polymeric surfaces would take only a certain amount of SMM.
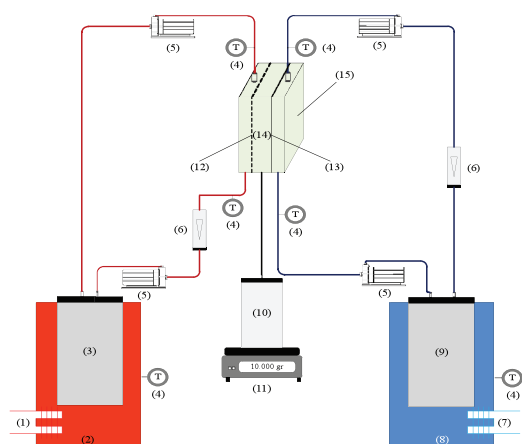

Fig. 2S. Schematic of AGMD experimental setup.
Note: (1) – Water heater, (2) – hot water bath, (3) – feed tank, (4) – thermocouple, (5) – peristaltic pump, (6) – flow meter, (7) – water cooler, (8) – cold water bath, (9) – cooling liquid, (10) – permeate tank, (11) – balance, (12) – membrane, (13) – cold plate, (14) – air gap and (15) – AGMD module.
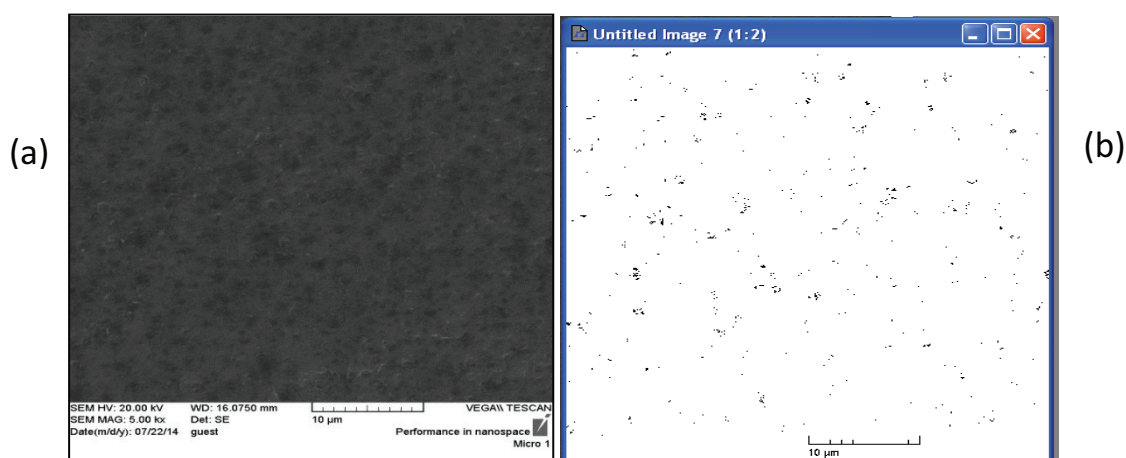

Fig. 3S. The influence of PVDF high concentration on decreasing of the porosity and pore size of the membrane surface: (a) SEM image and (b) image analyses of pore distribution on the surface of PVDF/SMM (20/1 wt%), without considering the evaporation time.

In fact, the saturation of surface take place in high SMM concentration. As a result, increasing of the SMM concentration up to these certain levels does not increase the percentage composition of the membrane surface anymore. In other words, the surface properties get independent from SMM in high concentration. In relevant works, it was seen that at SMM concentrations of about 2 wt%, the PVDF membrane surface is saturated. It was reported that the appropriate value of SMM concentration is around 0.5 wt%.

In this work, we employed two range of SMM concentrations as 2–4 wt% (in the 12 wt% PVDF and evaporation time of 1 min). Then the effects of SMM concentration changes on the membrane surface hydrophobicity were studied through water contact angle measurements. Results show that by twofold increasing in the SMM concentration (from 2 to 4 wt%), the significant changes in water CA of the membrane surface have not been seen. The correspondent CA images are represented at Fig. 4S.

2.6. Range of evaporation time

As mentioned, SMM migration occurs only in polymer solution, and migration stops after the phase separation process. As a result, prior to the coagulation, certain period of time is required for SMM migration to the surface of the membrane. Increase in the casting bath temperature and evaporation time, both strongly affect the SMM migration from the membrane bulk to surface. However, CA analyses indicate that after a period of elapsed time during the evaporation the SMM concentration in the membrane surface does not change (Fig. 5S). In this manner, the water contact angle of the membrane surface gets fixed because of the saturation of the surface with SMM. In addition, the increase in the evaporation time results in the thickening of the membrane skin layer. This results in the low porosity of the membrane. Moreover, the formation of skin layer diminishes the surface roughness and pore size as well as hydrophobicity.

Here for evaluating the influence of evaporation times on the surface hydrophobicity and porosity, two types of membranes were prepared in the various times of evaporation (6 and 8 min). The water CA and porosity measurements were conducted for both types of membranes. It was observed that by increasing the evaporation time from 6 up to 8 min, there is no delectable variations in the water CA values. However, the porosity of the membrane surface strongly decreased due to increasing in the thickness of formed skin layer.

3. Box–Behnken design

Response surface methodology (RSM) was applied in the variables and their independent and concert responses on the surface features. To achieve this goal, the three-level three-factorial Box–Behnken experimental design was chosen for finding out the relationship between the response functions (contact angle, pore size and overall porosity) and variables (PVDF concentration, SMM concentration and solvent evaporation time).

Independent variables and their levels for the Box–Behnken design used in this study are shown in Table 2S.

The second-order polynomial equation could be used to define the behavior of the system as follows:
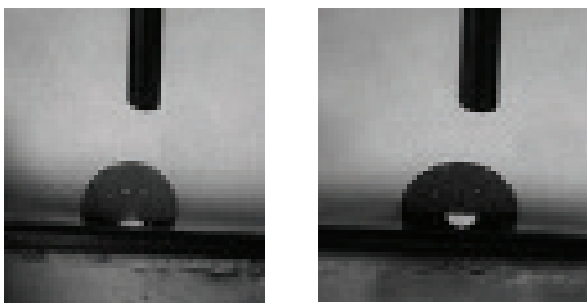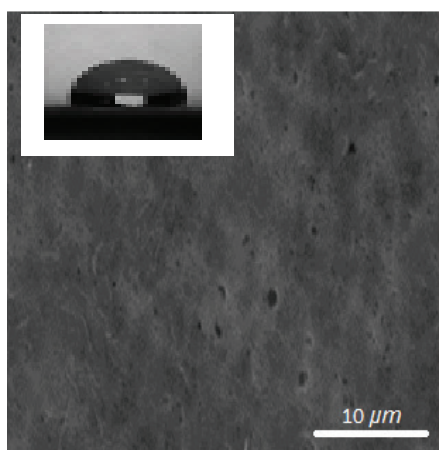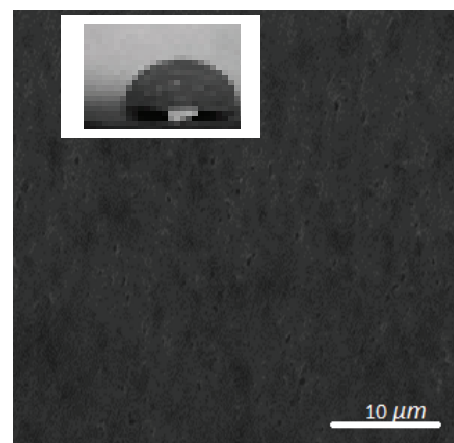

Fig. 4S. Water contact angle images of 12 wt% PVDF membranes: (a) 4 wt% of SMM, CA = 110°, and (b) 2 wt% of SMM, CA = 112°.

(a)   (b)

Fig. 5S. Surface contact angle and morphology of as prepared membranes: (a) for 6 min of evaporation time: ε = 73% and CA = 108° and (b) for 8 min of evaporation time ε = 69% and CA=106° (ε and CA stand for porosity and water contact angle, respectively).

$$Y = \beta_0 + \sum_{i=1}^{k} \beta_i x_i + \sum_{i=1}^{k} \beta_{ii} x_i^2 + \sum_{i=1}^{k-1} \sum_{j=2}^{k} \beta_{ij} x_i x_j + \varepsilon \qquad (4)$$

where Y stands for predicted responses (Y_1 is the surface contact angle; Y_2 is the mean surface pore size and Y_3 is the overall porosity). In the case of present problem of three independent variables, Eq. (4) is simplified as follows:

$$Y = \beta_0 + \beta_1 x_1 + \beta_2 x_2 + \beta_3 x_3 + \beta_{11} x_1^2 + \beta_{22} x_2^2 + \beta_{33} x_3^2$$
$$+ \beta_{12} x_1 x_2 + \beta_{13} x_1 x_3 + \beta_{23} x_2 x_3 + \varepsilon \qquad (5)$$

where x_1, x_2 and x_3 stand for input variables; β_0 is a constant; β_1, β_2 and β_3 are linear coefficients; β_{11}, β_{22} and β_{33} are quadratic coefficients; β_{12}, β_{13} and β_{23} are interactions and ε is noise or error.

In the present work, a Box–Behnken statistical design with three factors and three levels was employed to fit second-order polynomial model which indicated that 13 experiments were required for this procedure (Table 3S). The Design-Expert software (version 9, Stat-Ease Inc., Minneapolis, USA) was used for model regression, plotted figures and

optimization. The p values of less than 0.05 were considered to be statistically significant.

3.1. Mathematical model and optimization of modified PVDF membranes

Response surface optimization is more advantageous than the traditional single parameter optimization as it saves time, space and raw material. Thirteen experiments were performed to investigate the effects of the PVDF concentration (x_1), SMM concentration (x_2), solvent evaporation time (x_3) and their interactions on the responses (Y_1: contact angle, Y_2: mean pore size and Y_3: porosity). Independent variables and their levels for the Box–Behnken design used in this study are shown in Table 2S.

Using the relationships in Table 2S, the actual levels of the variables for each of the experiments in the design matrix were calculated, and experimental results obtained are given in Table 3S.

The analysis of variance (ANOVA) for three responses was given in Table 4S. The p value higher than 0.95 was considered as the threshold of parameter elimination in the response model equation calculations. The significance of each coefficient was determined by p value. The p value less than 0.05 indicates that model terms are significant. It was determined that the quadratic model was acceptable for responses and R^2 and R^2_{adj} indicate good agreement with the experimental data. As mentioned before, all the following figures were plotted using Design-Expert software, and in all presented figures, the other factor was kept at level zero (medium level).

From experimental results, the second-order response functions representing responses can be expressed as a function of the PVDF concentration (x_1), SMM concentration (x_2) and the solvent evaporation time (x_3). Table 5S presents the relationship between responses (Y_1, Y_2 and Y_3), and variables were obtained for coded unit for three size fractions. The responses at any regime in the interval of our experiment design could be calculated from Eqs. (4) and (5).

Table 2S
The level of variables chosen for the Box–Behnken design

Variable	Symbol	Coded variable level		
		Low	Center	High
		−1	0	1
PVDF concentration (wt%)	X_1	12	15	18
SMM concentration (wt%)	X_2	0	1	2
Evaporation time (min)	X_3	0	3	6

Table 3S
Box–Behnken design with actual/coded values for three size fractions and results

Run no.	Actual and coded level of variables			Experimental responses		
	X_1 (wt%)	X_2 (wt%)	X_3 (min)	Y_1 (°)	Y_2 (μm)	Y_3 (%)
1	18 (+1)	1 (0)	6 (+1)	112.52	0.11	67.85
2	12 (−1)	2 (+1)	3 (0)	112.86	0.14	78.50
3	15 (0)	2 (+1)	6 (+1)	115.00	0.12	67.70
4	18 (+1)	0 (−1)	3 (0)	86.50	0.15	74.50
5	18 (+1)	2 (+1)	3 (0)	110.61	0.11	70.60
6	12 (−1)	0 (−1)	3 (0)	86.20	0.23	82.04
7	15 (0)	2 (+1)	0 (−1)	107.80	0.13	80.42
8	18 (+1)	1 (0)	0 (−1)	102.30	0.12	74.64
9	15 (0)	1 (0)	3 (0)	105.25	0.15	76.40
10	12 (−1)	1 (0)	6 (+1)	114.77	0.14	75.28
11	12 (−1)	1 (0)	0 (−1)	103.41	0.19	83.43
12	15 (0)	0 (−1)	6 (+1)	86.25	0.18	72.50
13	15 (0)	0 (−1)	0 (−1)	86.00	0.19	79.64

Table 4S
Analysis of variance (ANOVA) quadratic model

Source	Contact angle (°)		Pore size (µm)		Overall porosity (%)	
	Regression coefficients	p value	Regression coefficients	p value	Regression coefficients	p value
Intercept	105.25		0.15		76.15	
X_1	−0.66	0.4961	−0.026	0.0006	−3.96	0.0005
X_2	12.66	0.0001	−0.031	0.0003	−1.43	0.0201
X_3	3.63	0.0150	−0.010	0.0196	−4.35	0.0003
X_1X_2	−0.64	0.6383	0.013	0.0290	−0.090	0.8760
X_1X_3	−0.28	0.8316	1.000E-002	0.0560	0.34	0.5640
X_2X_3	1.74	0.2385	2.944E-019	1.0000	−1.39	0.0615
X_1^2	1.64	0.3074	−3.750E-003	0.4216	0.25	0.7035
X_2^2	−7.85	0.0050	0.011	0.0550	0.012	0.9845
X_3^2	1.36	0.3874	−6.250E-003	0.2103	−1.10	0.1440

Table 5S
Model equations for contact angle, pore size and overall porosity

Responses	Model equation	Eq.	F value	p value	R^2	R^2_{adj}
Contact angle	$Y_1 = 105.25 − 0.66X_1 + 12.66X_2 + 3.63X_3 − 0.64X_1X_2 − 0.28X_1X_3 + 1.74X_2X_3 + 1.64X_1^2 − 7.85X_2^2 + 1.36X_3^2$	(6)	29.22	0.0027	0.9850	0.9513
Pore size	$Y_2 = 0.15 − 0.026X_1 − 0.031X_2 − 0.010X_3 + 0.013X_1X_2 + 1.000E-002X_1X_3 + 2.944E-019X_2X_3 − 3.750E-003X_1^2 + 0.011X_2^2 − 6.250E-003X_3^2$	(7)	31.34	0.0023	0.9860	0.9546
Porosity	$Y_3 = 76.15 − 3.96X_1 − 1.43X_2 − 4.35X_3 − 0.090X_1X_2 + 0.34X_1X_3 − 1.39X_2X_3 + 0.25X_1^2 − 1.10X_3^2$	(8)	29.01	0.0027	0.9849	0.9510